Experiments and Analysis for Composite Blades Under Large Deflections Part II: Dynamic Behavior

Pierre Minguet* and John Dugundji†
Massachusetts Institute of Technology, Cambridge, Massachusetts 02139

The dynamic behavior of structurally coupled composite blades is investigated in this paper analytically and experimentally, while the static behavior was described in Part I of this article. The model developed there is linearized around a given static position to investigate the small amplitude vibrations of composite blades. The influence coefficients method is used together with a simple iterative finite-difference solution procedure to obtain a standard eigenvalue problem. Several experiments using thin, flat composite cantilevered beams are also performed, and the data obtained compare well with the results from the analysis. The presence of static deflections is shown to have a significant influence on the torsion and fore-and-aft (lead-lag) modes and frequencies.

Introduction

FOLLOWING the description of the static behavior of composite blades in part I of this article,[1] their dynamic behavior is now presented. In order to be able to perform the aeroelastic stability analysis of a helicopter rotor, it is necessary to have an analytical model capable of predicting the blade natural frequencies and mode shapes. As mentioned in part I, most of the initial work on the subject focused first on obtaining a set of equations capable of describing the linear coupled bending and twisting behavior of nonuniform blades,[2,3] but it has been shown that nonlinearities caused by large displacements and rotations can be important in calculating the dynamic response and stability of rotor blades, especially when a hingeless configuration is used.[4,5] The traditional approach, retained here, obtains a set of linearized equations that can then be cast into a standard eigenvalue problem.[6-9] A linearized version of the model introduced in part I is presented here with an appropriate solution procedure. The results of several experiments using thin composite beams are presented also, and compared with the results from the analytical model. More detailed analytical and experimental results from this study can be found in Ref. 10.

Small Vibration Model

In part I of this article, a model was presented to study the large-deflection behavior of a structurally coupled blade under static loads. Here, after having determined the deformed position of a blade with that previous model, the next problem is to determine the blade's natural vibration frequencies and mode shapes around that position. Since one of the main points of interest in this study is the influence of static deformation on the vibration of blades, it is necessary to develop a model that accounts for the static large deflections of beams, instead of just considering a straight cantilevered beam. Again, all of the structural couplings must be accounted for, but for simplicity only small amplitude vibrations are considered.

This last assumption allows us to simply linearize the equations developed in part I by using the usual perturbation technique of replacing each quantity by its average value, plus a small perturbation whose squares are negligible:

$$F_k \to \bar{F}_k + F_k \tag{1a}$$

$$M_k \to \bar{M}_k + M_k, \quad k = 1, 2, 3 \tag{1b}$$

$$\theta \to \bar{\theta} + \theta, \quad \beta \to \bar{\beta} + \beta, \quad \psi \to \bar{\psi} + \psi \tag{1c}$$

$$x \to \bar{x} + x, \quad y \to \bar{y} + y, \quad z \to \bar{z} + z \tag{1d}$$

In all of the following, F_k, M_k, θ, β, ψ, x, y, z will now present force, moment, angle, and displacement perturbation values, whereas $\bar{F}_k$, $\bar{M}_k$, ... will represent average values. Note that all displacement and angle perturbations are measured in the global coordinate system (Fig. 1). Using these formulas, for example, the first equilibrium equation given in part I transforms as

$$\frac{d[\bar{F}_1 + F_1]}{ds} - [\bar{\omega}_\zeta + \omega_\zeta][\bar{F}_2 + F_2] + [\bar{\omega}_\eta + \omega_\eta][\bar{F}_3 + F_3] + \ldots = 0 \tag{2}$$

Applying these substitutions to all of the equations developed in part I, a new set of linear, first-order differential equations is obtained (with each linearized equation much longer than its original nonlinear version). Note that stress-strain relations were already linear and therefore do not change.

First, we obtain three force equilibrium equations

$$\frac{dF_1}{ds} - \bar{\omega}_3 F_2 + \bar{\omega}_2 F_3 - \bar{F}_2\omega_3 + \bar{F}_3\omega_2 + p_1^L + \bar{T}_{11}p_1^G + \bar{T}_{12}p_2^G + \bar{T}_{13}p_3^G + T_{11}\bar{p}_1^G + T_{12}\bar{p}_2^G + T_{13}\bar{p}_3^G = 0 \tag{3a}$$

$$\frac{dF_2}{ds} + \bar{\omega}_3 F_1 - \bar{\omega}_1 F_3 + \bar{F}_1\omega_3 - \bar{F}_3\omega_1 + p_2^L + \bar{T}_{21}p_1^G + \bar{T}_{22}p_2^G + \bar{T}_{23}p_3^G + T_{21}\bar{p}_1^G + T_{22}\bar{p}_2^G + T_{23}\bar{p}_3^G = 0 \tag{3b}$$

$$\frac{dF_3}{ds} - \bar{\omega}_2 F_1 + \bar{\omega}_1 F_2 - \bar{F}_1\omega_2 + \bar{F}_2\omega_1 + p_3^L + \bar{T}_{31}p_1^G + \bar{T}_{32}p_2^G + \bar{T}_{33}p_3^G + T_{31}\bar{p}_1^G + T_{32}\bar{p}_2^G + T_{33}\bar{p}_3^G = 0 \tag{3c}$$

and three moment equilibrium equations

$$\frac{dM_1}{ds} - \bar{\omega}_3 M_2 + \bar{\omega}_2 M_3 - \bar{M}_2\omega_3 + \bar{M}_3\omega_2 + m_1^L + \bar{T}_{11}m_1^G + \bar{T}_{12}m_2^G + \bar{T}_{13}m_3^G + T_{11}\bar{m}_1^G + T_{12}\bar{m}_2^G + T_{13}\bar{m}_3^G = 0 \tag{4a}$$

Received April 13, 1989; revision received Aug. 7, 1989. Copyright © 1989 by the American Institute of Aeronautics and Astronautics, Inc. All rights reserved.

*Research Assistant, Technology Laboratory for Advanced Composites, Department of Aeronautics and Astronautics.

†Professor, Department of Aeronautics and Astronautics. Member AIAA.

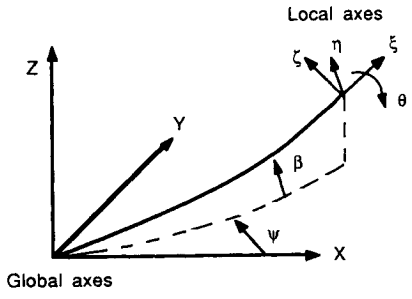

Fig. 1 Global and local axes.

$$\frac{dM_2}{ds} + \bar{\omega}_3 M_1 - \bar{\omega}_1 M_3 + \bar{M}_1 \omega_3 - \bar{M}_3 \omega_1 - F_3 + m_2^L + \bar{T}_{21} m_1^G + \bar{T}_{22} m_2^G + \bar{T}_{23} m_3^G + T_{21} \bar{m}_1^G + T_{22} \bar{m}_2^G + T_{23} \bar{m}_3^G = 0 \quad (4b)$$

$$\frac{dM_3}{ds} - \bar{\omega}_2 M_1 + \bar{\omega}_1 M_2 - \bar{M}_1 \omega_2 + \bar{M}_2 \omega_1 + F_2 + m_3^L + \bar{T}_{31} m_1^G + \bar{T}_{32} m_2^G + \bar{T}_{33} m_3^G + T_{31} \bar{m}_1^G + T_{32} \bar{m}_2^G + T_{33} \bar{m}_3^G = 0 \quad (4c)$$

followed by three curvature-angle compatibility equations

$$\frac{d\theta}{ds} = \omega_\xi - \cos\bar{\theta} \tan\bar{\beta}\, \bar{\omega}_\eta \theta - \frac{\sin\bar{\theta}}{\cos^2\bar{\beta}} \bar{\omega}_\eta \beta - \sin\bar{\theta} \tan\bar{\beta}\, \omega_\eta + \sin\bar{\theta} \tan\bar{\beta}\, \bar{\omega}_\xi \theta - \frac{\cos\bar{\theta}}{\cos^2\bar{\beta}} \bar{\omega}_\xi \beta - \cos\bar{\theta} \tan\bar{\beta}\, \omega_\zeta \quad (5a)$$

$$\frac{d\beta}{ds} = \sin\bar{\theta}\, \bar{\omega}_\eta \theta - \cos\bar{\theta}\, \omega_\eta + \cos\bar{\theta} \omega_\xi \theta + \sin\bar{\theta}\, \omega_\zeta \quad (5b)$$

$$\frac{d\psi}{ds} = \frac{\cos\bar{\theta}}{\cos\bar{\beta}} \bar{\omega}_\eta \theta + \sin\bar{\theta} \frac{\sin\bar{\beta}}{\cos^2\bar{\beta}} \bar{\omega}_\eta \beta + \frac{\sin\bar{\theta}}{\cos\bar{\beta}} \omega_\eta - \frac{\sin\bar{\theta}}{\cos\bar{\beta}} \bar{\omega}_\zeta \theta + \cos\bar{\theta} \frac{\sin\bar{\beta}}{\cos^2\bar{\beta}} \bar{\omega}_\xi \beta + \frac{\cos\bar{\theta}}{\cos\bar{\beta}} \omega_\zeta \quad (5c)$$

and three displacement-angle compatibility equations

$$\frac{dx}{ds} = -\sin\bar{\beta} \cos\bar{\psi}\beta - \cos\bar{\beta} \sin\bar{\psi}\psi \quad (6a)$$

$$\frac{dy}{ds} = -\sin\bar{\beta} \sin\bar{\psi}\beta + \cos\bar{\beta} \cos\bar{\psi}\psi \quad (6b)$$

$$\frac{dz}{ds} = \cos\bar{\beta}\beta \quad (6c)$$

Finally, we need also the linearized form of the transformation matrix

$$T_{11} = -\sin\bar{\beta} \cos\bar{\psi}\beta - \cos\bar{\beta} \sin\bar{\psi}\psi \quad (7a)$$

$$T_{12} = -\sin\bar{\beta} \sin\bar{\psi}\beta + \cos\bar{\beta} \cos\bar{\psi}\psi \quad (7b)$$

$$T_{13} = \cos\bar{\beta}\beta \quad (7c)$$

$$T_{21} = -\cos\bar{\psi} \cos\bar{\theta}\psi + \sin\bar{\psi} \sin\bar{\theta}\theta - \cos\bar{\theta} \sin\bar{\beta} \cos\bar{\psi}\theta - \sin\bar{\theta} \cos\bar{\beta} \cos\bar{\psi}\beta + \sin\bar{\theta} \sin\bar{\beta} \sin\bar{\psi}\psi \quad (7d)$$

$$T_{22} = -\sin\bar{\theta} \cos\bar{\psi}\, \theta - \cos\bar{\theta} \sin\bar{\psi}\psi - \cos\bar{\theta} \sin\bar{\beta} \sin\bar{\psi}\theta - \sin\bar{\theta} \cos\bar{\beta} \sin\bar{\psi}\beta - \sin\bar{\theta} \sin\bar{\beta} \cos\bar{\psi}\psi \quad (7e)$$

$$T_{23} = \cos\bar{\theta} \cos\bar{\beta}\theta - \sin\bar{\theta} \sin\bar{\beta}\beta \quad (7f)$$

$$T_{31} = \cos\bar{\theta} \sin\bar{\psi}\theta + \sin\bar{\theta} \cos\bar{\psi}\psi + \sin\bar{\theta} \sin\bar{\beta} \cos\bar{\psi}\theta - \cos\bar{\theta} \cos\bar{\beta} \cos\bar{\psi}\beta + \cos\bar{\theta} \sin\bar{\beta} \sin\bar{\psi}\psi \quad (7g)$$

$$T_{32} = -\cos\bar{\theta} \cos\bar{\psi}\theta + \sin\bar{\theta} \sin\bar{\psi}\psi + \sin\bar{\theta} \sin\bar{\beta} \sin\bar{\psi}\theta - \cos\bar{\theta} \cos\bar{\beta} \sin\bar{\psi}\beta - \cos\bar{\theta} \sin\bar{\beta} \cos\bar{\psi}\psi \quad (7h)$$

$$T_{33} = -\sin\bar{\theta} \cos\bar{\beta}\theta - \cos\bar{\theta} \sin\bar{\beta}\beta \quad (7i)$$

Once again, as in the static case, a system of 12 first-order differential equations is obtained. For the dynamics problem, we only need to add inertia loads to complete the equations. Since both the static and linearized part of the displacements are measured in global axes, these inertia loads will appear also as loads described in global axes, that is

$$p_1^G = -m\ddot{x} \quad (8a)$$

$$p_2^G = -m\ddot{y} \quad (8b)$$

$$p_3^G = -m\ddot{z} \quad (8c)$$

$$m_1^L = -I_p \ddot{\theta} \quad (8d)$$

where m is the blade mass per unit length and I_p the polar moment of inertia. Note that no rotary inertia terms have been used, these are usually negligible for most practical cases. If necessary, it would not be difficult to add these terms in the present formulation.

Several solution procedures would be available at this point, such as an assumed modes or energy method. In order to maintain some continuity with the static part of the problem, the same solution procedure used there is adopted. The beam is first divided into a series of discrete points or nodes and centered finite-difference formulas are used to discretize the equations just obtained. The influence coefficients method is then used to obtain the final form of the equations and construct the flexibility matrix [C] (i.e., the inverse of the stiffness matrix) in the following way.

1) For a given loading, the static problem is solved to determine the average "bar" values of all forces and displacements.

2) A unit load (in global axes) is applied at each node on each degree of freedom of interest, here the linearized displacements x, y, z, θ, with the displacement vector q arranged as

$$q = (\ldots, x^i, y^i, z^i, \theta^i, \ldots)^T \quad (9)$$

3) Using the iterative procedure described for the static model, linearized displacements and angles are determined and fill a column of [C] corresponding to the applied unit load.

$$\begin{bmatrix} \cdot \\ \cdot \\ x^i \\ y^i \\ z^i \\ \theta^i \\ \cdot \\ \cdot \end{bmatrix} = \begin{bmatrix} & & \\ & C_{ij} & \\ & & \end{bmatrix} \begin{bmatrix} 0 \\ 0 \\ \cdot \\ \cdot \\ 1 \\ 0 \\ \cdot \\ \cdot \end{bmatrix} \quad (10)$$

4) A diagonal lumped mass matrix is formed to represent inertia load

$$[M] = \text{diag}\,(\ldots, m\Delta s, m\Delta s, m\Delta s, I_p \Delta s, \ldots) \quad (11)$$

where Δs is the distance between nodes (uniformly spaced), except for the first and last node where it is half that value.

5) An eigenvalue problem is formulated by writing first

$$q = [C]f = -[C][M]\ddot{q} \tag{12}$$

Substituting

$$q = [M]^{-1/2} Xe^{i\omega t}$$

and premultiplying by $[M]^{+1/2}$ give the final form

$$X = [M]^{1/2}[C][M]^{1/2}\omega^2 X \quad \text{or} \quad \lambda X = [A]X \quad \text{with} \quad \lambda = \frac{1}{\omega^2} \tag{13}$$

6) This eigenvalue problem can then be solved by any classical method, such as Jacobi's method, to find all eigenvalues or the subspace iteration method to find only the first few eigenvalues.

Experiments

Several types of experiments were used to verify the analytical models presented here. As in part 1, several flat beam specimens were manufactured from AS4/3501-6 graphite/epoxy. These specimens were then tested dynamically to determine their natural vibration frequencies and mode shapes.

During the vibration tests, the blades were cantilevered in the same test fixture as for the static tests. As illustrated in Fig. 2, an electromagnetic shaker was placed underneath and connected to the blade with a soft spring. The shaker was connected to a variable frequency generator through an amplifier. One of the strain gauges, either an axial gauge for bending modes or a 45 deg gauge for torsion modes, was connected to an oscilloscope through a gauge box. A low-pass filter is also recommended during the tests to remove unwanted high-frequency noise. The signal from the frequency generator was also displayed on the second channel of the oscilloscope.

The goal of the tests was to identify the frequency of the first few natural vibration modes of each specimen. To do that, a frequency sweep was accomplished, starting at around 1 Hz, until a resonant mode was obtained. We can identify such a mode in several ways, for instance by noting a maximum in the amplitude of the beam displacements or gauge response. Also, at resonance, the signal of the gauge is roughly 90 deg out-of-phase with the signal from the frequency generator. Another possibility is to feed the signal from the frequency generator in place of the time signal of the oscilloscope and the gauge signal on the vertical channel to create Lissajou figures. A resonance is then indicated by a thin ellipse pattern on the screen of the oscilloscope. When a beam is tuned to a resonant frequency, node lines can be observed by sprinkling salt on the specimen surface and allowing it to collect at the nodes.

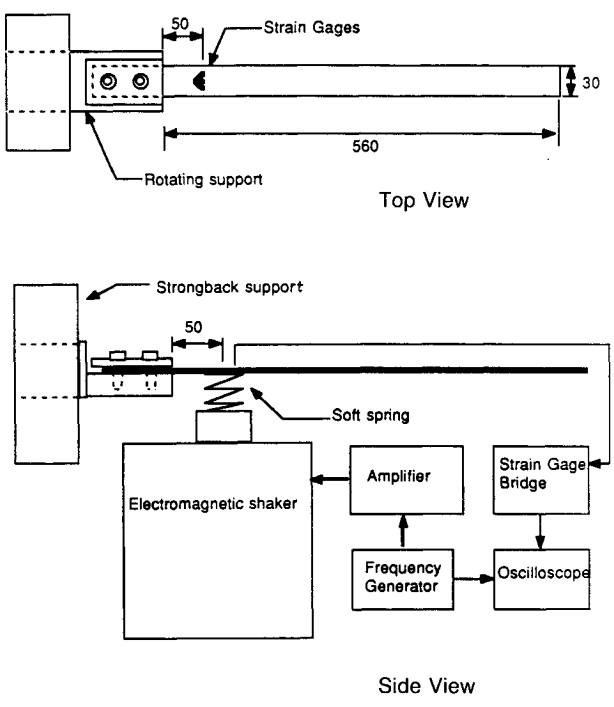

Fig. 2 Dynamic test setups.

Vibration Tests Results

In addition to obtaining actual blade vibration modes, another goal of the vibration tests was to observe two different types of effects: 1) the influence of the structural couplings created by the use of laminated composite structures, 2) the influence of static deflections on the natural frequencies of cantilevered blades. For the first effect, different types of layups were used to illustrate different types of structural couplings. For the second effect, the blade's own weight was used to produce some initial deflections and by using blades of different thicknesses, various amounts of initial deflections were present in these specimens. Also, because of the residual strains from the manufacturing process, most specimens exhibited some form of initial bending curvature. Thus, by testing the specimen with its top face up and then down it was possible for most specimens to obtain two different amounts of static tip deflection, since in one case the deflection due to the weight added up with the initial thermal deflection, while in the other case it was subtracted. Unlike the tests shown in Ref. 11 where a tip mass was used to create deflections, the present method allows us to see the influence of the deflections alone without any influence of the added tip inertia on the natural frequencies.

The first group of specimens contained several flat beams of standard dimensions, 560 by 30 mm, made of "thick" laminates (12 or 16 plies) with the following layups: $[0/90]_{3s}$, $[45/0]_{3s}$, $[20/-70/-70/20]_{2a}$. The first layup is a useful reference since it does not have any coupling, the second one has a fairly strong bending-twist coupling, and the last one has some extension-twist coupling. All of these specimens were fairly straight and did not deflect very much under their own weight, with tip deflections ranging from 10–20 mm.

During these tests, different types of vibration modes can be observed. There are the classical flapping (i.e., bending around the weak axis) modes. Then, for these relatively straight beams, two other types of vibration modes are present: a motion mostly in the horizontal plane that is a bending mode around the blade strong axis and is referred to as the fore-and-aft (or lead-lag) mode, and a classical torsion mode where the beam reference axis does not move significantly but twists around itself. The natural frequencies for these beams are summarized in Table 1. For this first group of specimens, however, no frequency is reported for the fore-and-aft mode because these beams are too stiff in that direction to get enough excitation from the shaker to observe any clear resonance. Also, the torsion mode is often much more difficult to identify since it is less easy to excite than the bending mode. It is interesting to compare the torsional frequencies of the different layups. As expected, the presence of 45 deg plies increases the torsional stiffness. Note that the $[20/-70/-70/20]_{2a}$ layup is thicker than the other two. For a simple comparison with the $[0/90]_{3s}$ and $[45/0]_{3s}$ specimens, frequencies can be scaled linearly with the thickness, i.e., by 12/16, giving a first bending frequency of 4.4 Hz and a first torsion frequency of 125 Hz, which compare favorably with the frequencies of the other two layups.

The next group of specimens contained three thinner speci-

Table 1 Experimental natural frequencies

Laminate[a]	Tip w_t,[b] mm	1B,[c] Hz	2B,[c] Hz	3B,[c] Hz	1T,[d] Hz	1F,[c] Hz
$[0/90]_{3s}$	20	5.7	34	98	62	___
$[45/0]_{3s}$	18	4.3	28	78	135	___
$[20/-70/-70/20]_{2a}$	12	5.8	36	103	166	___
$[0/90/0]_s$	15	3.1	19	54	89	___
	54	3.1	19	53	82	21
$[45/0/45]_s$	37	2.3	13	39	118	___
	101	2.3	13	38	101	17
$[20/-70/-70/20]_a$	9	3.0	18	50	111	___
	59	3.0	18	50	117	35
$[0/90]_s$	64	2.2	13	38	54	11
	163	2.3	13	37	46	5.6
$[45/0]_s$	137	1.4	8.0	20	68	10
	202	1.4	8.2	20	57	6.5

[a]Beam layup. [b]Tip deflection. [c]Frequency of bending mode. [d]Frequency of torsion mode. [e]Frequency of fore-and-aft mode.

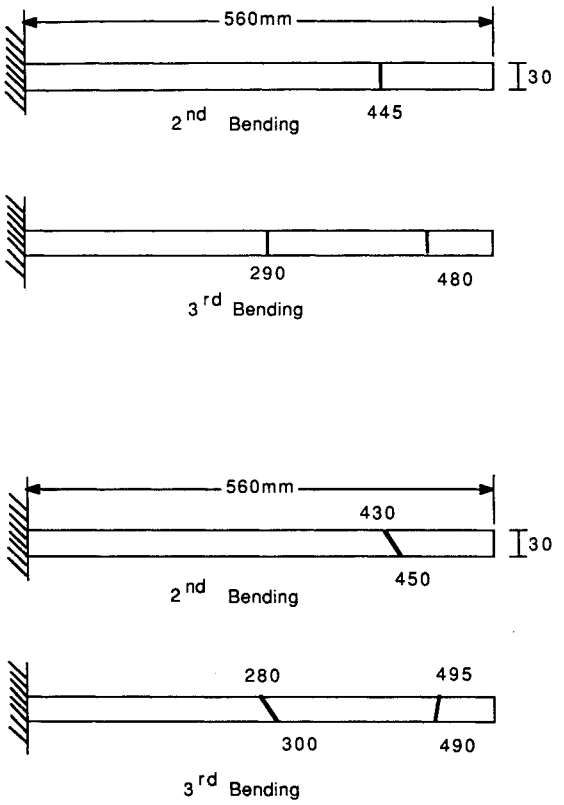

Fig. 3 Node line position for $[0/90/0]_s$ and $[45/0/45]_s$ beams.

mens, either six or eight plies thick, with layups of $[0/90/0]_s$, $[0/45/0]_s$, and $[20/-70_2/20]_a$. Their measured natural frequencies are also indicated in Table 1. The position of the node lines for some of these beams was recorded during the tests, and some examples are shown in Fig. 3. The influence of the bending-twist is clearly visible by the orientation of the node lines. Unlike the preceding group of specimens, all of these beams have some measurable deflections under their own weight. Therefore, as just explained, each specimen can be tested twice with two different amounts of tip deflection. The comparison between the two entries for each specimen shows that the bending modes do not appear to be affected by the beam deflection. The torsion mode however appears to be affected, with its frequency increasing in one case and decreasing in the other two. Also, when the deflections are sufficiently large, a fore-and-aft mode was clearly identified at a relatively low frequency. When deflections were smaller, however, this mode could not be identified and it is assumed that its frequency was too high to be measured, as seen in Table 1.

Table 2 Beam material properties

$[0/90]_{3s}$ laminate		
$t = 1.49\times10^{-3}$ m		
$m = 0.0683$ kg/m	$I_p = 5.13\times10^{-6}$ kg/m	
$E_{11} = 3.7\times10^{6}$ N	$E_{22} = 0.26\times10^{6}$ N	$E_{33} = 2.9\times10^{5}$ N
$E_{44} = 0.183$ Nm^2	$E_{55} = 0.707$ Nm^2	$E_{66} = 276$ Nm^2
$[45/0]_s$ laminate		
$t = 0.54\times10^{-3}$ m		
$m = 0.0238$ kg/m	$I_p = 1.66\times10^{-6}$ kg/m	
$E_{11} = 1.3\times10^{6}$ N	$E_{22} = 0.27\times10^{6}$ N	$E_{33} = 1.0\times10^{5}$ N
$E_{44} = 0.0195$ Nm^2	$E_{55} = 0.0143$ Nm^2	$E_{66} = 99.0$ Nm^2
$E_{12} = 0.9\times10^{5}$ N	$E_{45} = 0.00632$ Nm^2	

Note: In more conventional terms: $E_{11} \approx EA$, $E_{22} \approx GA_b$, $E_{33} \approx GA_c$, $E_{44} \approx GJ$, $E_{55} \approx EI_b$, $E_{66} \approx EI_c$, $E_{12} \approx$ extension-shear coupling, $E_{14} \approx$ extension-twist coupling, $E_{45} \approx$ bending-twist coupling.

The last group of specimens consisted of two thin, four-ply laminates, with layups of $[0/90]_s$ and $[45/0]_s$. These specimens were very flexible and much more sensitive to small manufacturing defects that can cause some residual thermal curvature. Again, as shown in Table 1, an increase in static deflections does not appear to affect the bending modes, their frequency, or mode shape. However, the torsion and fore-and-aft are strongly affected because both frequencies decrease as deflections increase. The mode shapes are also very different from those of a straight beam because in the fore-and-aft mode, the beam tip tends to swing laterally like a pendulum and twist near its root. In the torsion mode, the beam mean line moves only slightly around its rest position and the cross-section twists around that line.

Analysis of Results

The small amplitude vibration model developed earlier was checked against the experimental data. We compared the val-

Table 3 Experimental and analytical natural frequencies

Layup	Type	w_t, mm	1B, Hz	2B, Hz	3B, Hz	1T, Hz	1F, Hz
$[0/90]_{3s}$	Exp.	20	5.7	34	98	64	___
	Ana.	0	5.7	36	101	84	113
	Ana.	20	5.7	36	101	68	126
$[45/0]_s$	Exp.	137	1.4	8.0	20	68	10
	Ana.	0	1.3	8.0	22	48	115
	Ana.	137	1.3	8.0	22	61	11
	Exp.	202	1.4	8.2	20	57	6.5
	Ana.	202	1.3	7.9	22	55	7.5

ues of the natural frequencies to verify the data.

As a first example, the natural frequencies of a straight $[0/90]_{3s}$ specimen (i.e., with no tip deflection, $w_t = 0$) are calculated using the properties shown in Table 2, and the results are given in Table 3. Note that these values would be obtained using classical beam theory since there are no structural couplings and the beam is straight. As one can see, the agreement with the experiment is very good for the first three bending modes, but not very good for the torsion mode. As a second example, the frequencies calculated for a $[45/0]_s$ beam with zero tip deflection are also shown in the same table. Once again, the agreement with the experiment is good for the bending modes, but the value of the torsion mode frequency is completely different from the experimental value.

Calculations for other specimens show the same trend of good agreement with the experiment for the bending frequencies, but very poor correlation for the torsion mode frequencies. The reason for this discrepancy is the presence of static deflections in all of the specimens tested. A new set of calculations were then performed to take this effect into account; a small uniform load is applied on the beam (in the analysis) to obtain some static tip deflection, and new frequencies are then calculated. The results, shown in Table 3, are interesting, even for the 12-ply-thick specimen which barely deflects under its own weight. The presence of a small tip deflection can have a significant effect on the torsion frequency. For instance, for the $[0/90]_{3s}$ beam with a 20-mm tip deflection (compared with a 560-mm specimen length), the calculated torsion frequency drops from 84 to 64 Hz. For the $[45/0]_s$ specimen with a 137-mm tip deflection, the torsion frequency goes up from 48 to 61 Hz, which compares well with the experimental data.

These two preliminary examples illustrate quite well that the static (small or large) deflection of the beam can have a strong influence on the natural frequencies. In order to investigate that influence further, several beams were analyzed in some detail and several analyses of each beam are performed. All of the material properties used in these calculations are indicated in Table 2.

In all of the results next presented, 16 nodes were used to discretize the beam, with four degrees of freedom at each node. The computer program was run on a DEC MicroVax II computer, and each load case required about 15 s of CPU time for the static solution and between 50 and 150 s of CPU time for the dynamic solution, the longer times corresponding to cases with large deflections and strong structural couplings. In each case, the procedure is the same: a given uniform distributed load is applied on the beam, the static position is calculated, the tip deflection noted as a reference, and the natural frequencies and mode shapes are then calculated for that position.

The first beam to be studied is the $[0/90]_{3s}$ specimen since it has no couplings and will only show the effect of large deflections. In Fig. 4, some of the mode shapes for a straight beam are shown as a reference. Note in this figure and the following ones, that the θ component of the mode shapes has been multiplied by the chord of the beam c in order to compare θ with the other three components u, v, w. As we can see, these are very classical shapes for the first three bending, fore-and-aft, and torsion vibration modes. Notice particularly the frequency of the torsion mode at 84 Hz and of the fore-and-aft mode at 113 Hz.

A small, uniformly distributed load is then applied to this beam, resulting in a tip deflection of about 11 mm (2% of the beam length), and the new mode shapes are plotted in Fig. 5. The bending modes show little change, both in frequency and in shape, but a small u component is now coupled with w. However, for the torsion and fore-and-aft modes, the change is quite dramatic. What was the torsion mode now has a strong v component coupled in and the frequency is down to 77 Hz, and what was the fore-and-aft mode has a strong θ component, with its frequency going up to 119 Hz. In the first case, the v and θ components are in opposite phase, while in

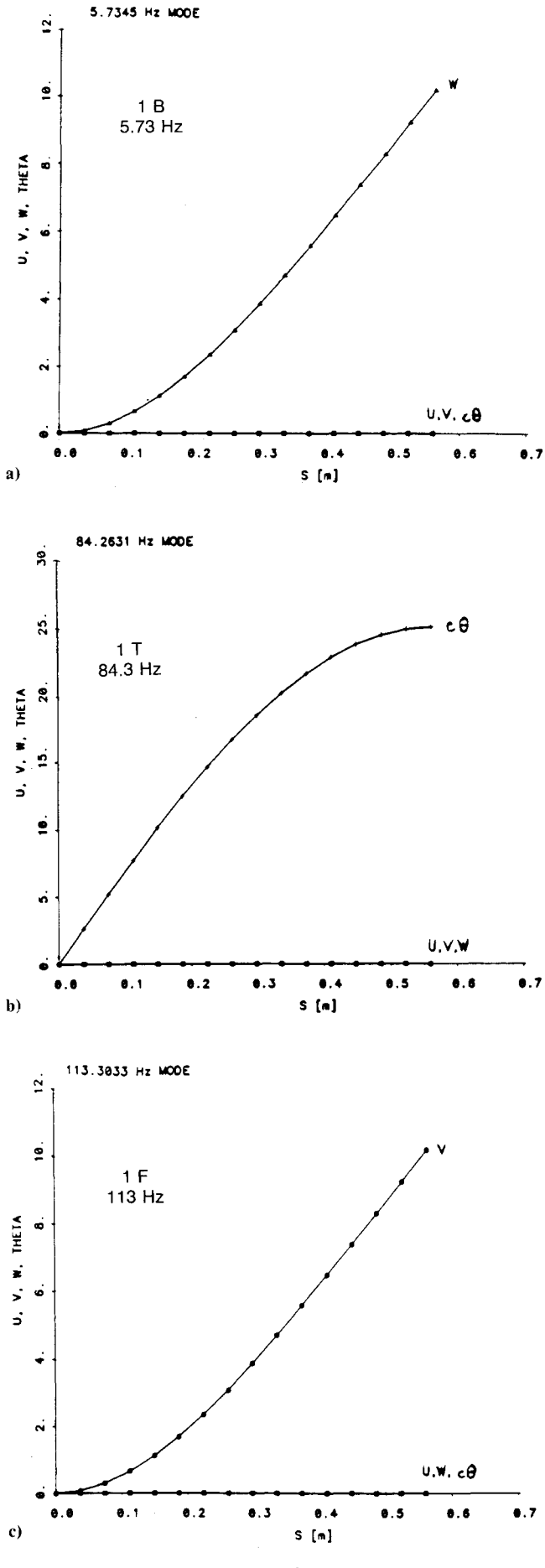

Fig. 4 Vibration modes for $[0/90]_{3s}$ beam with no tip deflection.

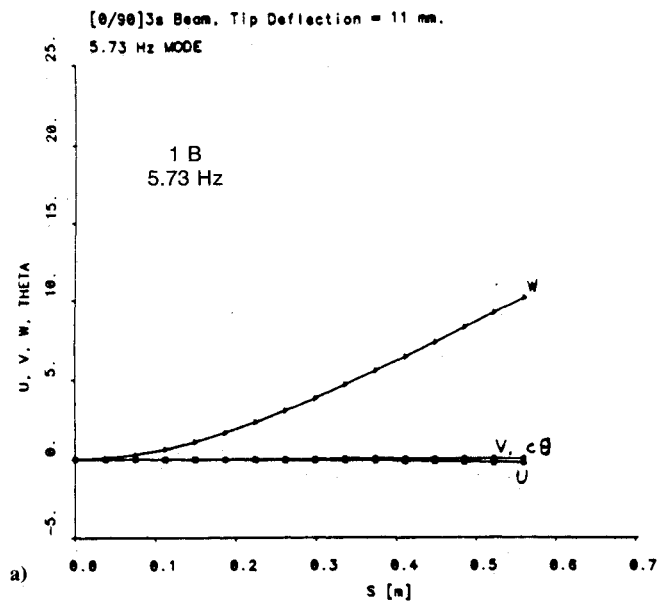

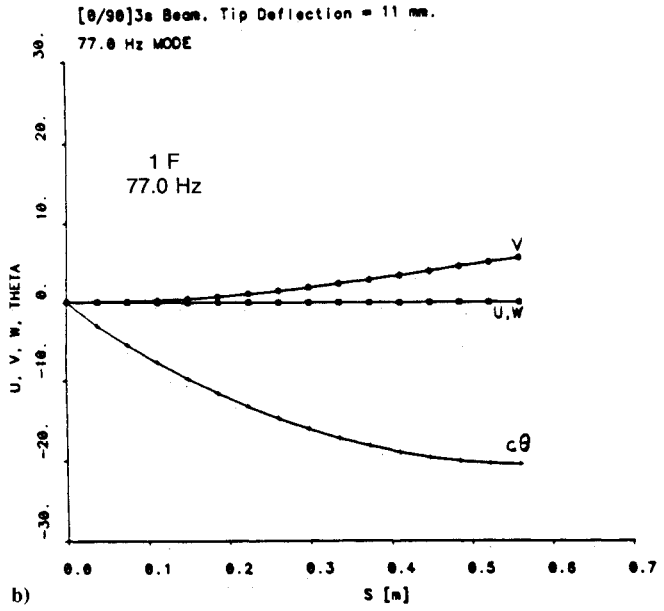

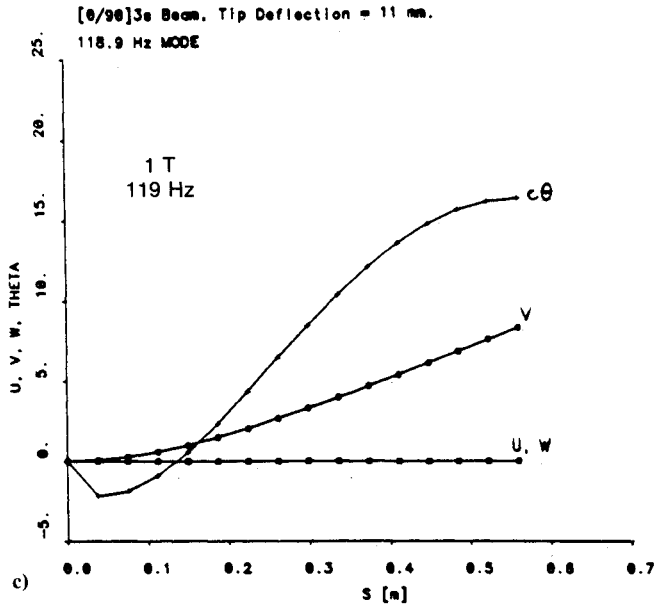

Fig. 5 Vibration modes for $[0/90]_{3S}$ beam with a tip deflection of 2% of its length.

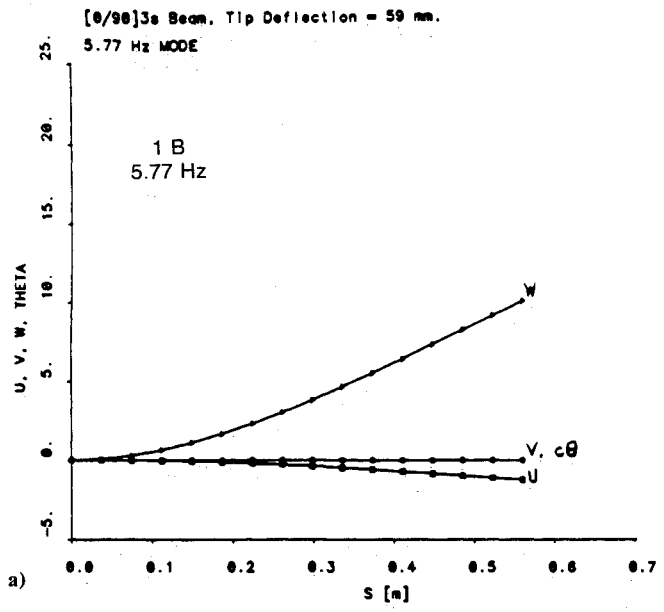

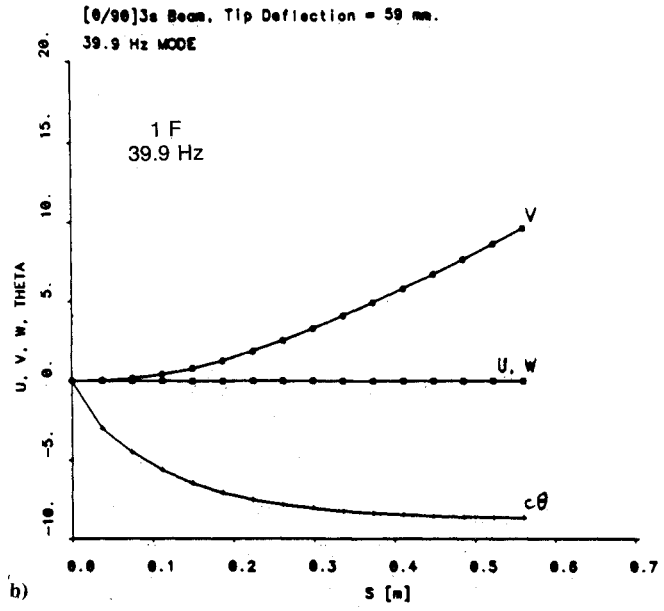

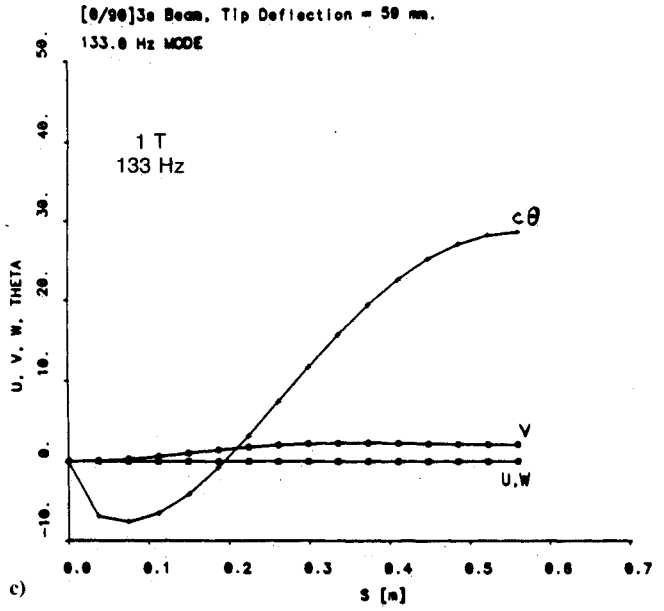

Fig. 6 Vibration modes for $[0/90]_{3S}$ beam with a tip deflection of 11% of its length.

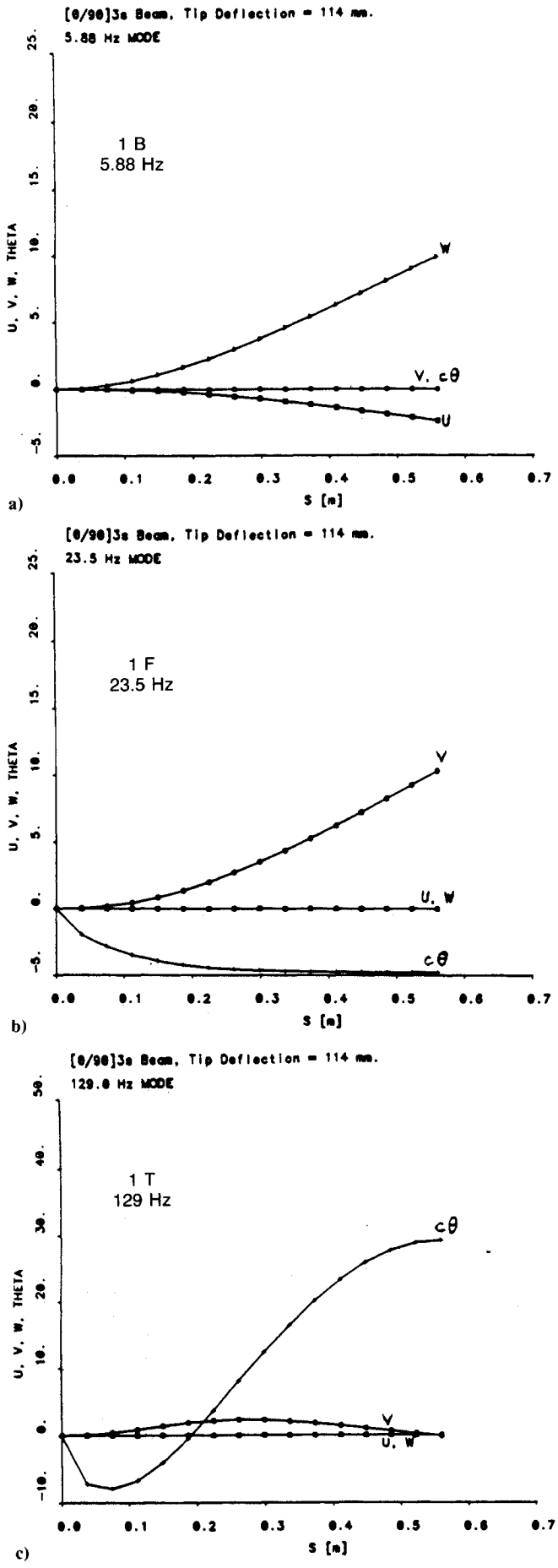

Fig. 7 Vibration modes for $[0/90]_{3s}$ beam with a tip deflection of 20% of its length.

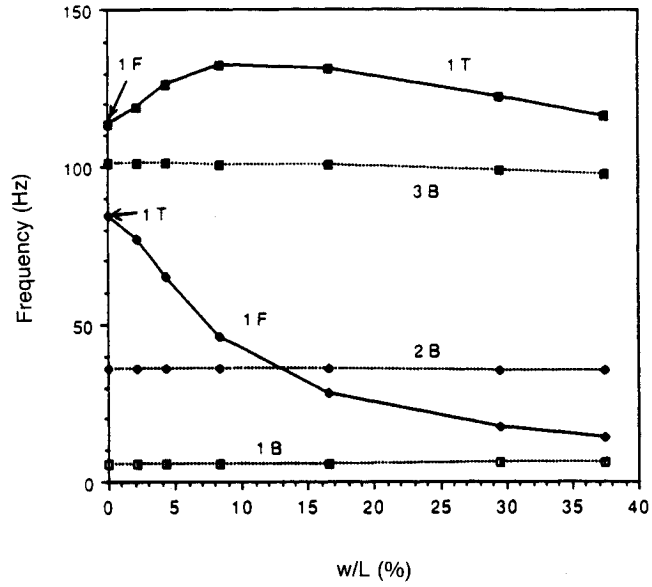

Fig. 8 Changes in natural frequencies for $[0/90]_{3s}$ beam with increasing tip deflection.

the second case, they are in phase. It should be noted generally that, for negative static tip deflections (i.e., due to gravity), all u and v components woul be the negative of those shown here.

The distributed load on the beam is then increased, giving a positive tip deflection of 59 mm (11% of the length), and the resulting mode shapes are shown in Fig. 6. Once again, the bending mode frequencies do not change significantly, and there is now a larger u component in the modes. The torsion mode has now gone down to 40 Hz and become mostly a fore-and-aft mode, while the fore-and-aft mode has gone up to 133 Hz and become mostly a torsion mode. Thus, one can say that as the deflections increase, these two modes gradually "exchange" their shapes.

The results for a further increase in load, giving a tip deflection of 114 mm (20% of the length), are shown in Fig. 7. The frequency of the fore-and-aft mode is down to 23.5 Hz, and the mode shape consists mostly of a v displacement with most of the twist concentrated near the root of the beam. The "torsion" mode frequency has slightly decreased from the preceding case to 129 Hz. Its shape looks somewhat like a second torsion mode with a small v displacement. Finally, the results for a 210-mm deflection (37.5% of the length) are calculated. The same qualitative observations as in the preceding cases can be made about the mode shapes. The fore-and-aft frequency is down to 14 Hz and the torsion frequency is slightly down at 116 Hz.

The preceding changes in frequencies for the $[0/90]_{3s}$ beam with an increasing tip deflection are summarized in Fig. 8, where 1B, 2B, 3B are the first three bending modes, 1F the first fore-and-aft, and 1T the first torsion modes. The most interesting facts to notice are the interaction between the fore-and-aft and torsion modes, and how relatively small amount of deflections can affect their frequencies.

The next beam illustrated here is the $[45/0]_s$ specimen, which shows the influence of bending-twist coupling. Calculations are first done for a straight beam and, as expected, all the bending modes contain a twist component. The torsion and fourth bending mode, at 48.7 and 44.4 Hz, respectively, couple together because their frequencies are relatively close. As in the preceding specimen, the magnitude of the transverse load is then gradually increased to give static tip deflections,

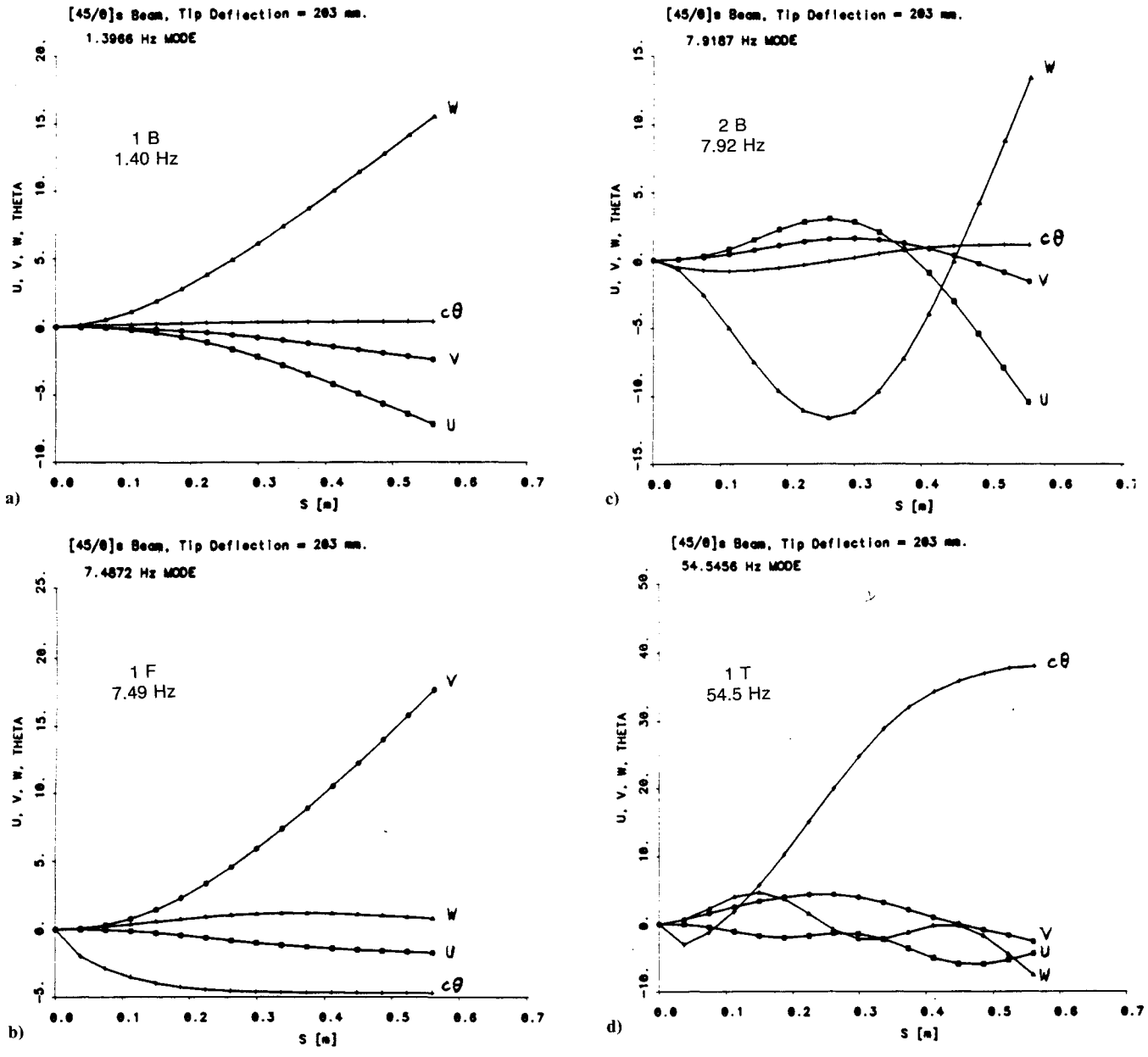

Fig. 9 Vibration modes for $[45/0]_s$ beam with a tip deflection of 36% of its length.

and the changes in frequencies are noted. Only the last case is shown in Fig. 9, for a tip deflection of 204 mm, which was actually present in one of the test specimens. As one can see, these modes have become quite complex and sometimes can be difficult to interpret. Note how the first bending mode is coupled with a fore-and-aft component, and how the fore-and-aft and second bending modes are all coupled because their frequencies are relatively close (from 7.5–7.9 Hz) and because of the bending-torsion coupling. The first torsion mode is also strongly coupled to other displacements, and the $[0/90]_{3s}$ specimen has more of a second torsion mode shape. Finally, the evolution of the frequencies with tip deflection is summarized in Fig. 10. A comparison with the experimental values is also shown in Table 3. The agreement for most frequencies is good, with a little more error for the torsion mode. One should note, however, that in the analysis there were several modes with a strong torsion component between 60–80 Hz and that identifying which one can be called the first torsion mode may not be clear.

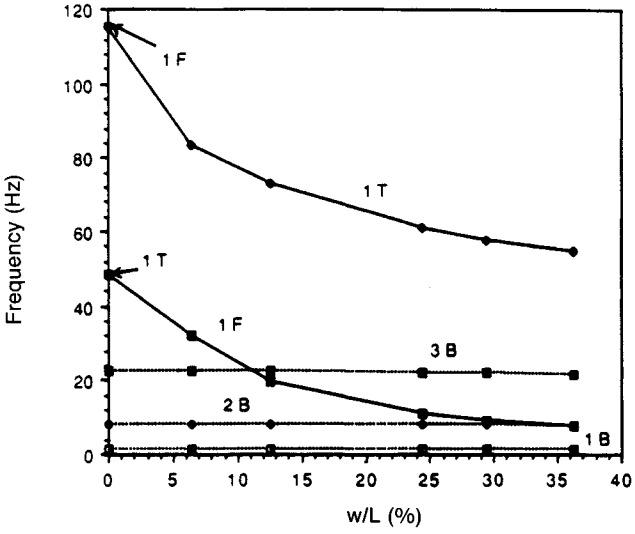

Fig. 10 Changes in natural frequencies for $[45/0]_s$ beam with increasing tip deflection.

Conclusion

A new analytical model based on the use of Euler angles and a fast and efficient solution procedure has been presented. Geometric nonlinearities are taken into account exactly for the static behavior and then linearized for the study of small amplitude vibrations. All material couplings such as bending-torsion and extension-torsion are also taken into account easily. Several experiments using thin, flat, composite cantilevered beams were also performed, and the data obtained compared well with the results of the analysis. Both experimental and analytical results show that the presence of static deflection can significantly reduce the frequency of the fore-and-aft mode and also strongly influence the torsion mode.

Acknowledgments

This research was supported by U.S. Army Research Office Contract DAAL03-87-K-0024, with Gary Anderson as Technical Monitor. Many thanks also to Adam Sawicki and Michael Sadlowski for their help with the experimental part of this project.

References

[1]Minguet, P. J., and Dugundji, J., "Experiments and Analysis for Composite Blades Under Large Deflections Part I: Static Behavior," *AIAA Journal,* Vol. 28, No. 9, 1990.

[2]Houbolt, J. C., and Brooks, G. W., "Differential Equations of Motion for Combined Flapwise Bending, Chordwise Bending, and Torsion of Twisted Non-Uniform Rotor Blades," NACA Rept. 1346, 1958.

[3]Isakson, G., and Eisley, J. G., "Natural Frequencies in Coupled Bending and Torsion of Twisted Rotating and Nonrotating Blades," NASA CR-65, July 1964.

[4]Friedmann, P. P., "Recent Developments in Rotary-Wing Aeroelasticity," *Journal of Aircraft*, Vol. 14, No. 11, 1977, pp 1027–1041.

[5]Friedmann, P. P., "Recent Trends in Rotary-Wing Aeroelasticity," *Vertica,* Vol. 11, No. 1/2, Jan. 1987.

[6]Hong, C. H., and Chopra, I., "Aeroelastic Stability of a Composite Rotor Blade," *Journal of the American Helicopter Society,* Vol. 30, No. 2, April 1985.

[7]Bauchau, O. A., and Hong, C.-H., "Finite Element Approach to Rotor Blade Modelling," *Journal of the American Helicopter Society,* Vol. 32, No. 1, Jan. 1987.

[8]Hodges, D. H., and Dowell, E. H., "Nonlinear Equations of Motion for the Elastic Bending and Torsion of Twisted Non-Uniform Rotor Blades," NASA TN D-7818, Dec. 1974.

[9]Hinnant, H. E., and Hodges, D. H., "Nonlinear Analysis of a Cantilever Beam," *AIAA Journal,* Vol. 26, No. 12, 1988.

[10]Minguet, P. J., "Static and Dynamic Behavior of Composite Helicopter Rotor Blades Under Large Deflections," Ph.D. Thesis, Dept. of Aeronautics and Astronautics, Massachusetts Institute of Technology, May 1989; also TELAC Rept. 89-7, M.I.T, May 1989.

[11]Dowell, E. H., and Traybar, J., "An Experimental Study of the Non-Linear Stiffness of a Rotor Blade Undergoing Flap, Lag and Twist Deformations," Princeton Univ., Princeton, NJ, AMS Rept. 1257, Dec. 1975.

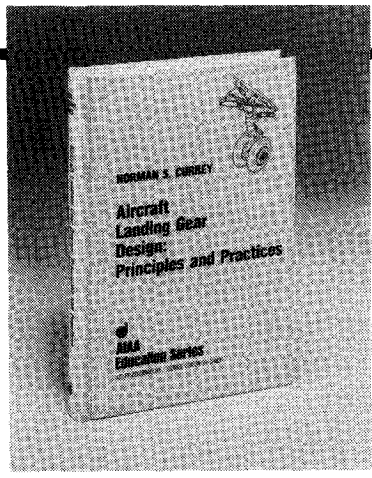

Aircraft Landing Gear Design:
Principles and Practices

by Norman S. Currey

The only book available today that covers military and commercial aircraft landing gear design. It is a comprehensive text that leads the reader from the initial concepts of landing gear design right through to final detail design. The text is backed up by calculations, specifications, references, working examples, and nearly 300 illustrations!

This book will serve both students and engineers. It provides a vital link in landing gear design technology from historical practices to modern design trends. In addition, it considers the necessary airfield interface with landing gear design.

To Order, Write, Phone, or FAX:

AIAA

c/o TASCO
9 Jay Gould Ct., P.O. Box 753, Waldorf, MD 20604
Phone (301) 645-5643 Dept. 415 FAX (301) 843-0159

AIAA Education Series
1988 373pp. Hardback
ISBN 0-930403-41-X

AIAA Members $42.95
Nonmembers $52.95
Order Number: 41-X

Postage and handling $4.75 for 1-4 books (call for rates for higher quantities). Sales tax: CA residents 7%, DC residents 6%. Orders under $50 must be prepaid. Foreign orders must be prepaid. Please allow 4 weeks for delivery. Prices are subject to change without notice.

945